Li *et al. Chin. J. Mech. Eng.* (2020) 33:97
https://doi.org/10.1186/s10033-020-00515-6

Chinese Journal of Mechanical Engineering

ORIGINAL ARTICLE Open Access

Sensitivity of Influential Factors on Needle Insertion Experiments: A Quantitative Analysis on Phantom Deformations and Needle Deflections

Murong Li, Yong Lei* and Tian Xu

Abstract

High repeatability of needle insertion experiments is essential to the needle-phantom interaction model validation. However, the influential factors governing the accuracy of the phantom and needle deformations have not been systematically studied. In this paper, the impact of influential factors, including phantom characteristic represented by the ratio of DMSO and thawing time (TT), needle properties represented by needle external diameter (NED) and operating factors such as needle insertion velocity (IV), insertion positions (IP) and repeated insertion times (RITs) are analyzed by orthogonal experiment design. The range calculation shows the most sensitive parameters to phantom deformations are RITs, IV and DMSO while the most sensitive parameters to needle deflection are DMSO, TT and NED. By variance analysis, the significant factors on maximum tissue deformation (MTD) are IV, followed by RITs, DMSO and IP. And NED and TT have nearly no significant impact on MTD. The significant sequence on maximum needle deflection (MND) is as follows: DMSO, TT and NED. Results show that, among all impacting factors, phantom deformation is susceptible to both material properties and operative factors while the needle deflection is more susceptible to material properties of the phantom, which can help researchers in related fields to conduct experiments in a more precise manner and better understand the needle-phantom interaction mechanism.

Keywords: Needle insertion, Sensitivity analysis, Tissue deformation, Needle deflection

1 Introduction

A slender puncture needle penetrating into an organ is widely used for extracting the pathological tissue of the organ or delivering drugs to the target areas in surgical operation, as shown in Figure 1. Such minimally invasive surgeries in biopsy, local anesthesia and brachytherapy had been widely studied [1–4]. Extensive work has been done to establish the needle-tissue interaction model to study the internal deformation, needle deflection and their interactions. The accuracy and reliability of the model relies on the experimental verification which require repeatable and accurate experiments.

In medical research, simulation experiments require the use of tissue-like objects that mimic the properties of human or animal tissues [5–7]. The tissue-mimic material is also required to be stable and transparent so the deformation information can be easily obtained. There are many kinds of phantom mimicking materials, such as carrageenan, gellan gum, and oil-in-gelatin dispersions [8–10]. The force-displacement curves, axial force magnitude, crack shape as well as the influence of operation in both phantom were compared with real organs [11, 12]. The tissue-mimic material is also required to be stable and transparent so the deformation information can be easily obtained. Among the numerous simulation

*Correspondence: ylei@zju.edu.cn
State Key Laboratory of Fluid Power & Mechatronic Systems, Zhejiang University, Hangzhou 310027, China

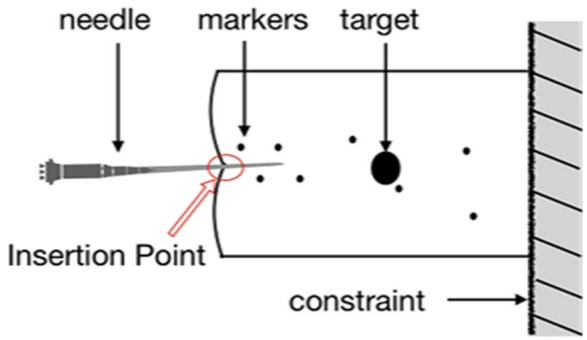

Figure 1 Needle insertion into the phantom in the center of one side

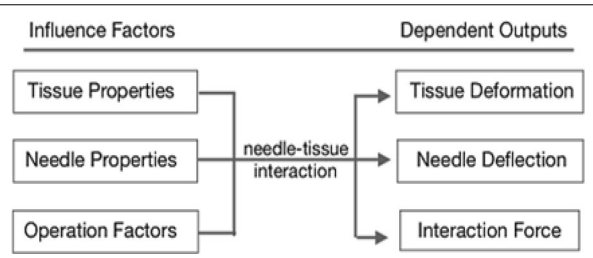

Figure 2 A schematic depiction of the influential factors that impact the results of phantom deformations, needle deflections and the interaction forces

materials, PVA hydrogel have been extensively used as a phantom material to mimic the mechanical behavior of the soft biological tissues [6, 13–15]. Jiang et al. [14] compared the deformation of PVA with the porcine liver by varying the freeze/thaw (FT) cycles of PVA hydrogel and found their similarity in both mechanical and morphological characteristics. The internal properties of PVA characterized by the interaction force were assessed with human tissues [8], which showed the friction-displacement slope would be larger with the increase of mass of PVA and FT cycles. Mano et al. [16] found an appropriate ratio of PVA and water to mimic the human soft tissue properties in MRI parameters. Jong et al. [6] study the suitability of polyvinyl alcohol (PVA) as a liver tissue mimicking material in terms of needle-tissue interaction, the studies found that the mechanical properties of PVA hydrogels can be influenced in a controlled manner by varying the concentration of PVA and the number of freeze-thaw cycles, to mimic liver tissue characteristics.

Figure 2 shows a schematic depiction of the influential factors that impact the phantom deformations, needle deflections and the interaction force. The influential factors can be divided into three groups: phantom properties, needle properties and the operation factors.

The operation factors represent how the needle intersects the soft phantoms, for instance, the insertion velocity, the insertion location and etc. In literature, needle insertion force modeling can be classified into the following categories: finite element methods [17], energy methods [18], statistical methods [19], and analytical methods (FEM) [20]. In this paper, we focus on the statistical methods based on the physical experimental data. Gerwen et al. [21] reviewed the experimental data with regards to the needle-phantom interaction forces and showed the effect of numerous factors such as needle type, insertion speed and phantom characteristics on the interaction force during different insertion phase. The survey indicated the axial force as well as the friction force increase with the velocity in artificial material and reduce with the axial rotation. Both in silicone and human tissues, it was found that puncture force increases with needle diameter, especially with a blunt needle tip. Jiang et al. [22] analyzed the effect of needle geometries, insertion methods and phantom characteristics on the needle-phantom interaction forces by remarking the factors based on the positive, negative or inconclusive correlation. Yang et al. [20] presented a survey that systematically summarizes the state-of-the-art force control technologies for robot-assisted needle insertion, such as force modeling, measurement, the factors that influence the interaction force, parameter identification, and force control algorithms. In Ref. [23], six different tips including beveled and conical versions, with or without pre-bend or pre-curve with a constant diameter were selected and studied. Compared to the conical tips, the beveled tips with increased tip angels tend to have a higher force-displacement slope. Some studies aimed to investigate the influence of needle locations on the interaction force by inserting needles into the different zones of the phantoms at different angle, but no obvious statistical significance of the insertion axial force was found [24, 25].

Other literature, though scarce, focused on the influence factors on the phantom deformations and needle deflections [26–28]. Swaney et al. [29] proposed a new flexure-based needle tip design that provided the enhanced steerability of kinked bevel-tip needles which can minimize tissue damage effectively. Alterovitz and Goldberg [26] developed an interaction model of needle insertion during radioactive seed implantation. The results indicated the physician-controlled parameters play an important role in the phantom movement while phantom properties, such as stiffness and compressibility have less effect on the seed placement. In Ref. [27], Misra et al. generated a FE mesh to study the deformations of phantoms and concluded that, rather than the material properties of phantom, the geometry of the tissues and boundary constraints dominated the response of phantom deformations. An analytical model used to calculate the needle-phantom interaction forces and

moments at a beveled tip was presented in Ref. [28], and both experimental and analytical results verified smaller bevel angle leads to larger transverse tip forces and larger needle deflection. Moshen et al. [30] studied the effect of insertion velocity on needle force, tissue deformation and needle work during the needle insertion procedures. The J intergal method and a nonlinear viscoelastic Kelvin model were applied to predict the rupture deformation and the results indicated that most of the benefits of using a higher needle speed can be achieved by using a finite speed that is inversely proportional to the relaxation time of the organization.

In Ref. [31], the existing experimental evidence regarding the influence of different factors was represented. A data model was constructed that described the interrelations between the different aspects of needle-tissue interaction experiments. The most important contribution of this work consists of a set of tools for gathering, analyzing, and disseminating experimental needle-tissue interaction data.

From the prior work, a substantial studies investigated the effects of phantom characteristics, needle geometry or the operation factors on the interaction force while the quantification of the influential factors on both phantom deformations and needle deflections were not thoroughly studied with experimental verification, and there is no enough statistical conclusion available on it. In this paper, the effects of three kinds of influential factors on both PVA phantom deformations and needle deflections are investigated through orthogonal experiments. The contribution of this paper can be summarized as follows: first, the effects of influential factors on the phantom deformations and needle deflections are jointly studied. Second, some other factors such as repeated insertion, the thawing time for phantom hydration are first mentioned and found to be influential on the phantom deformations and needle deflections, respectively. The results of the experiments can provide important data for parameter estimation and model verification, which can provide the guidance to researchers in related fields to better design needle insertion experiments.

The rest of the paper is organized as follows: Section 2 introduces the basic three phases of needle insertion experimental procedures, followed by the the orthogonal test design in Section 3. In Section 4, the experimental results including range calculations and variance analysis are presented. Finally, the discussion, conclusion and future work are shown in Section 5 and Section 6.

2 An Introduction of Needle Insertion Experiments

Figure 3 shows a diagram of needle insertion experiments procedures, including the preparation and maintenance of phantom, needle insertion procedures and data post-processing. The experimental testbed is constructed to drive the needle to insert into the phantom and record the phantom deformation and needle deflection.

2.1 Testbed Configuration

Figure 4 shows the testbed, which consists of a CCD camera, a tissue container, a needle clamper, a light source, a needle, two linear actuators and one rotator. The linear actuators (ML01.8A1, ML01.4A1, the resolution is 0.25 μm) are provided by Physik Instrument (PI Shanghai) Co. Ltd. The rotator (the resolution is 0.225 °)

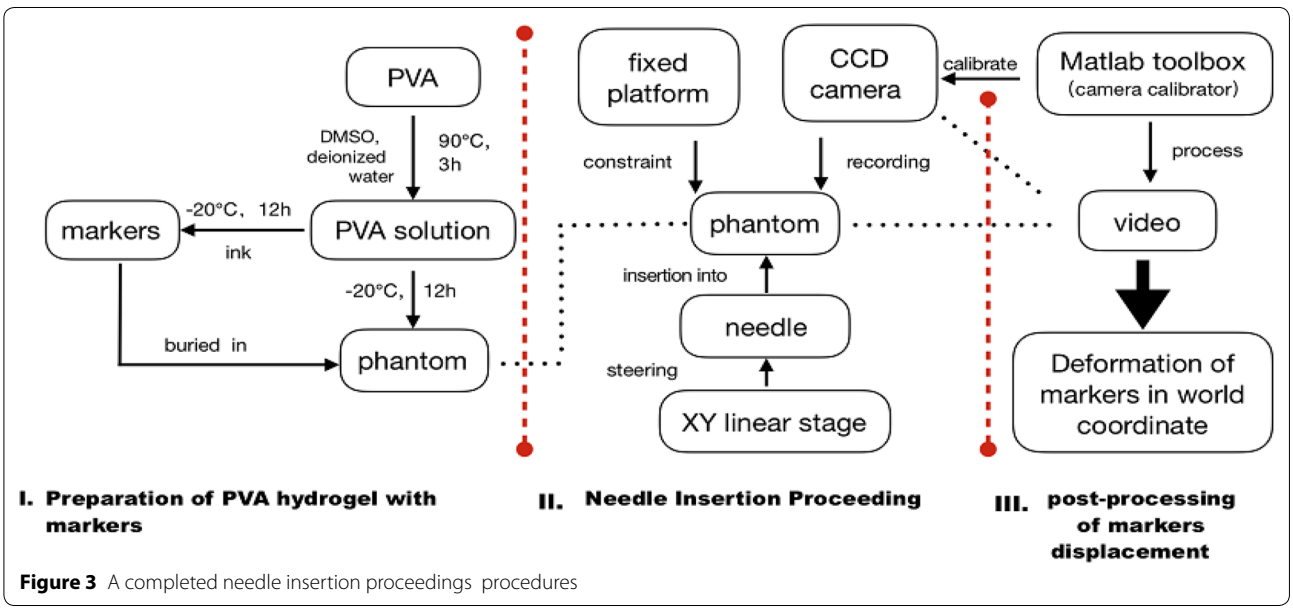

Figure 3 A completed needle insertion proceedings procedures

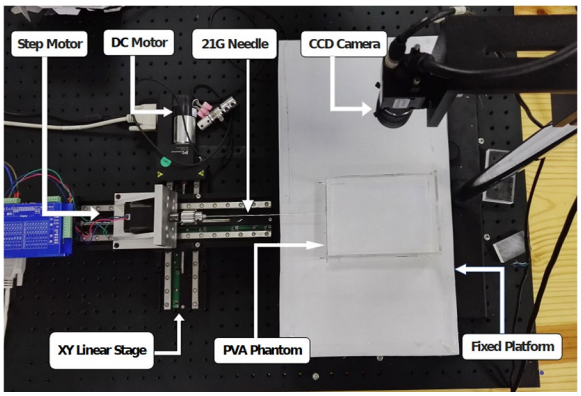

Figure 4 Experimental testbed for needle insertion procedures

is provided by HWHR Instruments Co. Ltd. A 18G–22G PTC needle (the diameter of solid needle is 0.71–1.26 mm, and the tip is with bevel angle of 20°) with a plastic hub (provided by Bard Peripheral Vascular, Inc.) is fixed by the clamper. A 6 degree-of-freedom force sensor (ATI, Nano 17SI, the revolution is 0.0625 N) is amounted on the needle base to record the insertion force at 40 Hz. The computer obtains force sensing data through NI data acquisition board (PCI 6620). The sample of artificial tissue (phantom) is made of polyvinyl alcohol (PVA) and its size is 20 mm × 100 mm × 150 mm. The CCD camera (MV-EM510C/M, the revolution of picture is 2456 × 2058 and the pixel size is up to 3.45 × 3.45 μm) is provided to record the trajectory of needle and phantom's deformation. The frequency of image acquisition 3 pic/s.

2.2 Polyvinyl Alcohol (PVA) Hydrogel Preparation

The manufacturing of the PVA hydrogel is as follows: Dimethyl-sulfoxide(DMSO) is added into the mixture of PVA and de-ionized water, where DMSO is used as a solvent to improve the transparency and maintain certain mechanical properties of the gel. The material behavior is similar to the porcine liver [14, 15]. The stiffness of the phantom can be adjusted by changing the ratio of DMSO to water. The DMSO/water ratio ranges from 3/7 to 5/5 by volume and the mass of PVA/solvent keep 8 g/100 g correspondingly at each experimental group. Then the mixed solution configured is then stirred on a magnetic stirrer while heated at 90 °C untill the solution is homogeneous and transparent, after which, the solution is poured into an acrylic box employed with the volume of 150 mm×100 mm×20 mm. The acrylic box is then placed in the refrigerator at −20 °C for 12 h for crystallization. In order to avoid wrinkles and bubbles on the solution surface, the plastic wraps were covered on the box. Markers used for visualization of the phantom deformation are made of the dyed PVA hydrogel prepared in the same way and then crystallized in capillaries with diameter of 1 mm. After 12 h of crystallization, both of the phantom and the markers are in solid state and the markers are then implanted in the phantom. A markers' template is utilized to ensure the position consistence in each phantom. The distribution of the markers is shown in Figure 5.

To characterize the mechanical properties of PVA hydrogel with different ratio of DMSO, the standard tensile tests on PVA samples are shown in Figure 6. Three kinds of volume ratio of DSMO to water used are 3/7, 4/6, 5/5, respectively. The dumbbell shape of the samples is shown in Figure 6.

Nine groups of PVA gel were tested where the samples with the same proportioning were repeated three times. During the experiments, loading was in tensile mode and conducted on the PVA gel sample between two fixtures of stretching machine, the force and displacement relationship was recorded by the stretching machine at a tensile speed of 0.8 mm/s. The nine groups of experiments were carried out and the results was shown in Table 1. From

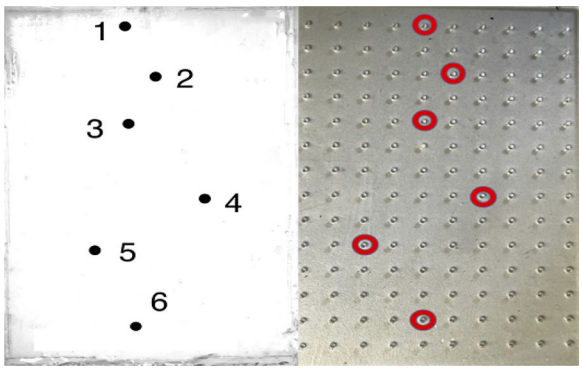

Figure 5 Tensile test of the PVA phantom

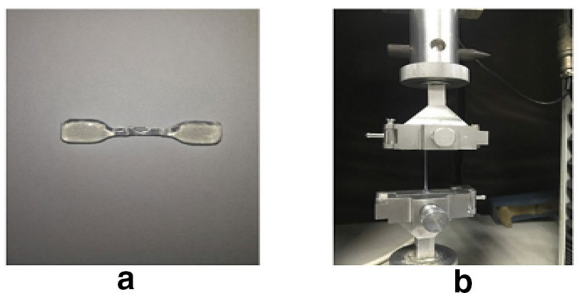

Figure 6 Distribution of markers buried in the phantom using markers' template

Table 1 Characteristic of PVA hydrogel

Ratio of DMSO to water	Young's modulus (kPa) (min, mean, max)
3/7	9.2, 11.9, 14.6
4/6	26.1, 29.8, 31.3
5/5	53.5, 55.4, 56.9

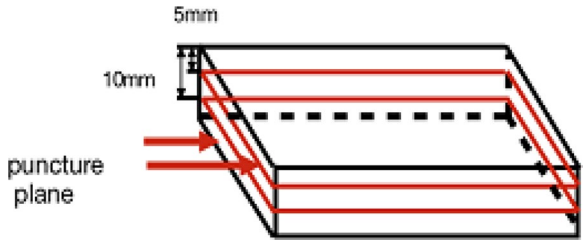

Figure 7 Different insertion positions

the Table 1, we can conclude that the Young's modulus of the PVA hydrogel increase with the ratio of DMSO. The Young's modulus of the PVA hydrogel ranges from 9.2 kPa to 56.9 kPa.

2.3 Needle Insertion Procedures

The test phase refers to having a needle inserted into the phantom fixed at the bottom surface at a constant velocity. Before the insertion procedures, the CCD camera is calibrated to establish the transform of the picture coordinate system to the world coordinate system. The relative position between the PVA phantom and needle was also be calibrated. As shown in Figure 4, needle is driven by the 3-DOF motion platform at a constant velocity, which would cause the phantom's internal deforming (characterized by markers movements). The insertion depth is 80 mm. Needle would also deflect under the unbalanced force acting on the beveled needle tip. The deformation of the phantom and deflection of needle were recorded by the CCD camera. The needle insertion point is in the center of the one side of phantom as shown in Figure 1. Needle insertion and markers recording are limited to the 2D plane. Hence, it is necessary to study the effect of different insertion positions (IP). Figure 7 shows a schematic diagram of different insertion positions which is defined by the distance between the insertion plane to the phantom surface. Other operation factors investigated in this paper include the needle insertion velocity (IV) and repeated insertion times (RITs) into the same trajectory. In practice, RITs may occur when the previous insertion failed and adding this factor helps us to understand if the repeated insertion would cause any difference in phantom deformations or needle deflections. In repeated insertion process, the needle was inserted into the same positions of the tissue immediately; Hence, we assumed this time interval between each insertion has no effect on the results of repeated insertion.

2.4 Postprocessing Phase

Needle deflection and phantom deformation together determine whether the needle could touch the target while avoiding the obstacles at the same time. Therefore, the concerned output of this research mainly focused on the results of needle deflection and phantom deformation. Phantom deformation is calculated by image processing technology to extract the areal coordinates of the six markers. In order to convert pixel coordinates to world coordinates, a step of calibration is implemented in advance [33]. As can been seen in the Figure 5, markers' position coordinates in each picture relative to the initial position (in the first picture) constituted the deformations of corresponding positions. Similarly, the postprocess of needle deflection is to track the needle tip position and calculate the ultimate tip's lateral deviation from the needle base.

3 Orthogonal Experimental Design

The orthogonal experimental design is applied to the sensitivity analysis of impacting factors of needle insertion owing to the advantages of short time, high yield and low cost results. In order to improve the repeatability of the experiments, the impacts of the possibly induced error is studied by one-at-a-time (OAT) sensitivity method in Ref. [29] and the results show there is no significance with a small variance of stirring temperature (ranging from 70 °C to 90 °C) and frozen time (ranging from 11 h to 13 h). However, during the interval between taking the phantom out of refrigerator to carrying insertion experiments which is termed as the thawing time (TT), the phantom is continuously dehydrated, which would change the properties of the phantoms. To author's knowledge, up to now there is no other studies investigating the effect of thawing time of phantoms or tissues. As a result, the influence of TT is added as one of the possible factors that affect the deformation results.

In this paper, the selected six influential factors are classified into three groups: phantom properties, needle properties and operation factors. The phantom properties include the volume percentage of DMSO to water (DMSO for short later) as well as the phantom hydration during thawing time (TT). The needle external diameter (NED) characterized by 'G' is the selected parameter for needle properties. As for operation factors, insertion velocity (IV), repeated insertion times (RITs) and insertion positions (IP) are chosen. The selection of factors

Table 2 Factors and levels

Factor	Factor level
Ratios of DMSO	{40%, 50%, 60%}
Thawing time (TT)	{1 h, 4 h, 7 h}
Needle external diameter (NED)	{18G, 20G, 22G}
Insertion velocity (IV)	{ 1 mm/s, 3 mm/s, 6 mm/s }
Repeated insertion times (RITs)	{1, 2, 3}
Insertion positions (IP)	{5 mm, 10 mm}

and their corresponding levels are in Table 2. In the meantime, it is emphasized that the temperature and humidity of the laboratory remain relatively stable during the thawing phase.

Figure 8 shows the trajectories of the six markers during one needle insertion experiment. In the figure, the displacement in the needle insertion direction (y) is much larger than the lateral direction (x). Hence, we mainly focus on the vertical displacement (y). Figure 9 depicts the relative maximum displacement of markers in y direction. 'p1' refers to the marker 1, which has the maximum displacement and can be used as a reference standard. The figure demonstrates that the relative displacements of markers are proportionate, hence, selecting any one of the marker's deformation results as experimental output would come to the same conclusion. For convenience, the displacement of 'p1' in the needle insertion direction(y) is chosen as one of the experimental output. As the needle deflection would increase with the insertion depth, the maximum needle deflection(MND), namely the deflection at insertion depth of 80mm is treated as the needle deflection output.

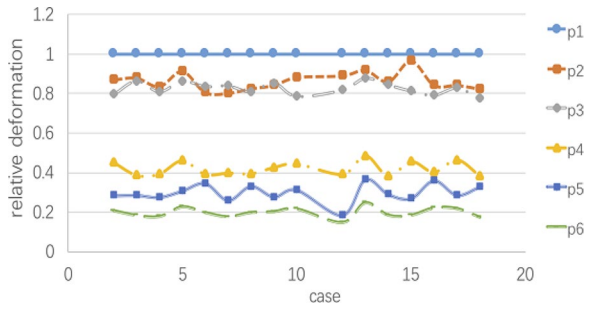

Figure 9 Relative displacement of markers in all cases

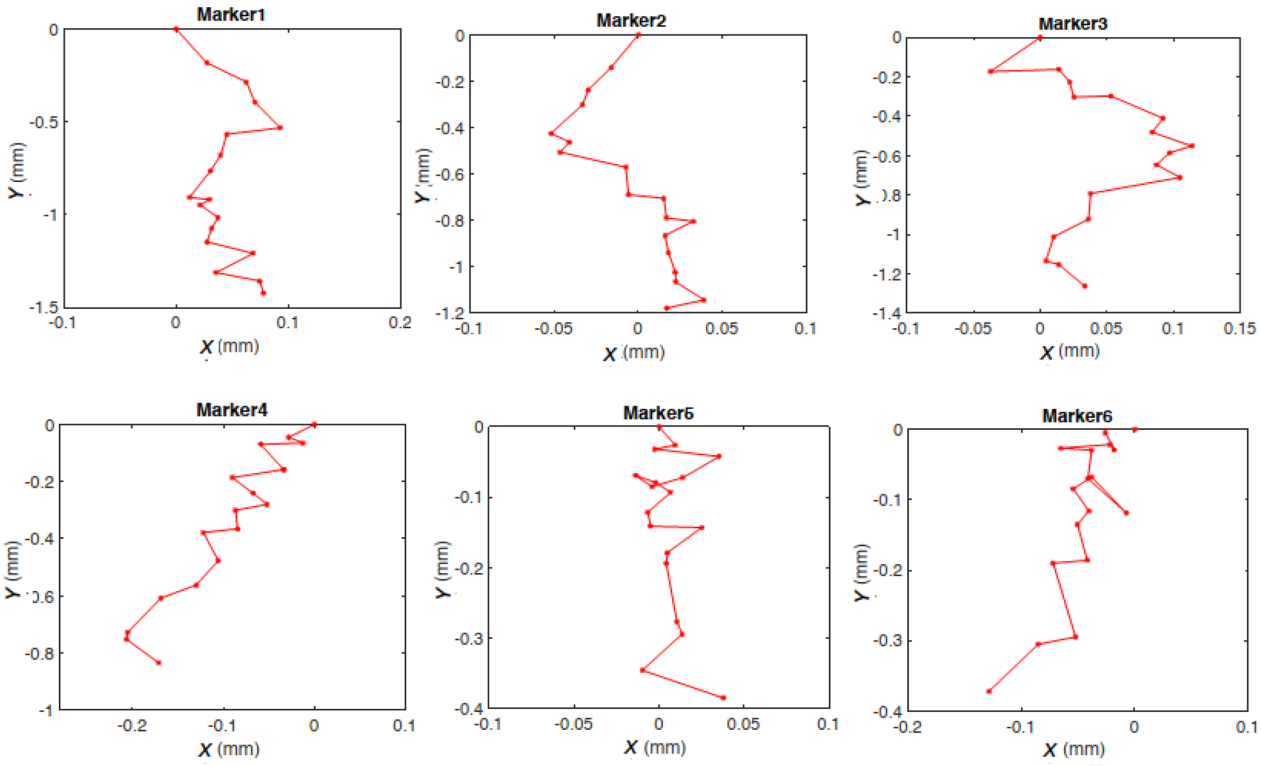

Figure 8 Trajectory of six markers during needle insertion

Table 3 Orthogonal test of input parameters and the corresponding results of MTD and MND

Cases	DMSO (%)	TT (h)	NED (G)	IV (mm/s)	RITs	IP	MTD (mm)	MND (mm)
1	40	1	18	1	1	p1	4.92	1.70
2	40	4	20	3	2	p1	6.64	2.28
3	40	7	22	6	3	p1	9.77	3.93
4	50	1	18	3	2	p1	10.06	3.27
5	50	4	20	6	3	p1	6.87	4.60
6	50	7	22	1	1	p1	2.76	6.60
7	60	4	18	6	1	p1	4.63	6.60
8	60	7	20	1	2	p1	3.16	8.00
9	60	1	22	3	3	p1	4.69	5.93
10	40	7	18	3	3	p2	9.33	3.60
11	40	1	20	6	1	p2	4.90	1.94
12	40	4	22	1	2	p2	2.77	2.84
13	50	4	18	1	3	p2	4.65	4.34
14	50	7	20	3	1	p2	2.50	5.73
15	50	1	22	6	2	p2	5.46	5.03
16	60	7	18	6	2	p2	5.34	6.94
17	60	1	20	1	3	p2	3.00	5.00
18	60	4	22	3	1	p2	2.56	8.50

4 Sensitivity Analysis Results of Needle Insertion Experiments

This section describes the results of global sensitivity analysis. Both range calculation and variance analysis are applied to the experimental data to find the influential degree of the selected factors.

4.1 Range Calculation Results

The above-mentioned parameters are placed into an orthogonal table in Table 3. It can be seen that 18 tests are used to arrange five factors with three levels and one factor with two levels. The experimental output MTD and MND are recorded in the last two column.

Average value and range calculation results of movements of needle and phantom are calculated in Table 4 and Table 5, respectively. It can be seen that the three of the most sensitive parameters to phantom deformations are RITs, IV and DMSO, followed by the NED, IP and the TT. The range calculation results of needle deflection show that the sensitivity ranking successively are DMSO, TT and NED. Other factors rarely affect the results of the needle deflection.

Figure 10 and Figure 11 plot the main effect of the factors within the selected range. The trends of the curves can explain the specific effect of each factor. As can be seen in Figure 10, the phantom's deformations increase as the ratio of the DMSO decrease because the stiffness of the phantom would become harder with the increase of DMSO.

Table 4 Average value and range calculation of MTD

Factor	Value	MTD (mm)	Range (mm)	Rank
DMSO (%)	40	6.39	2.50	3
	50	5.38		
	60	3.89		
TT (h)	1	5.50	0.82	6
	4	4.69		
	7	5.78		
NED (G)	18	6.49	1.98	4
	20	4.51		
	22	4.67		
IV (mm/s)	1	3.54	2.62	2
	3	5.96		
	6	6.16		
RITs	1	3.71	2.68	1
	2	5.57		
	3	6.39		
IP	p1	5.94	1.44	5
	p2	4.50		

Moreover, the phantom deforms more severely as the insertion velocity and the diameter of the needle increase which may induced by extra dynamic reaction. A second or third needle insertion in the same trajectory would cause a larger phantom deformations compared with the first insertion results.

Different from the factors affecting the phantom deformations, the needle deflection is more sensitive to

Table 5 Average value and range calculation of MND

Factor	Value	MTD (mm)	Range (mm)	Rank
DMSO (%)	40	2.72	4.11	1
	50	4.93		
	60	6.82		
TT (h)	1	3.81	1.98	2
	4	4.87		
	7	5.79		
NED (G)	18	4.41	1.05	3
	20	5.00		
	22	5.46		
IV (mm/s)	1	4.75	0.41	4
	3	4.89		
	6	4.84		
RITs	1	5.18	0.62	5
	2	4.74		
	3	4.56		
IP	p1	4.77	0.11	6
	p2	4.88		

the properties of the phantoms, as shown in Figure 11. Increase in the ratio of DMSO and lengthening the thawing time would have the phantom become harder, thus increasing the interaction force and causing a larger needle deflection. Needle's diameter would also affect the deflection degree in the way that the thinner the needle, the larger the needle deflection. As a result, choosing a thick needle would reduce the ultimate deviation of the needle tip.

4.2 Variance Analysis

The results of variance analysis are shown in Table 6 and Table 7 where SG represents the abbreviation of significance. Compared with F value of each parameter, the significant levels are represented by the symbol '*'. More '*' represent more significant impact on MTD or MND. From Table 6, the most significant factors on MTD are IV, followed by RITs, DMSO and IP. And NED and TT have nearly no significant impact on MTD. Variance analysis on MND shows the significant sequence is as follows: DMSO, TT and NED. Other factors should be considered as inapparent factors since $p > 0.1$.

The pareto chart of the significant parameters is shown in Figure 12 and Figure 13 based on the results of the range calculation and variance analysis. It can be seen that the ratio of DMSO impact both MTD and MND. Apart from this, the operation factors such as RITs, IP or IV significantly impact the results of phantom

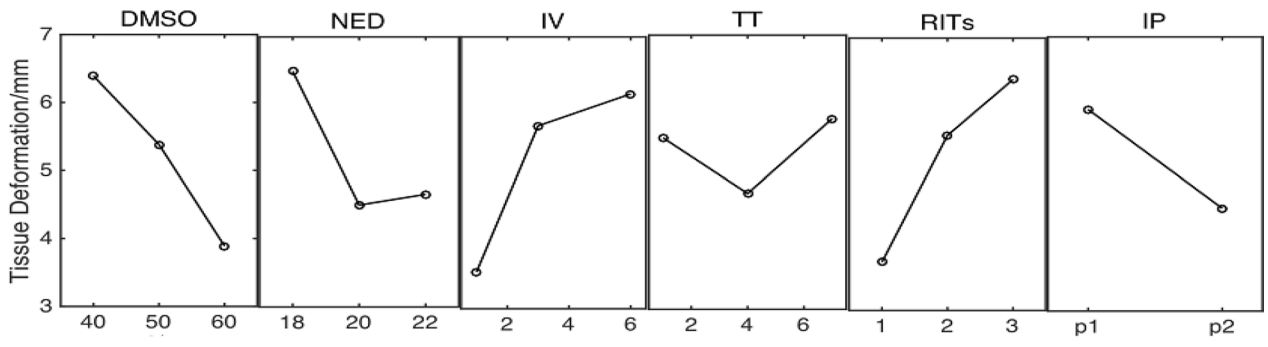

Figure 10 Main effect plot of orthogonal factor on phantom deformations

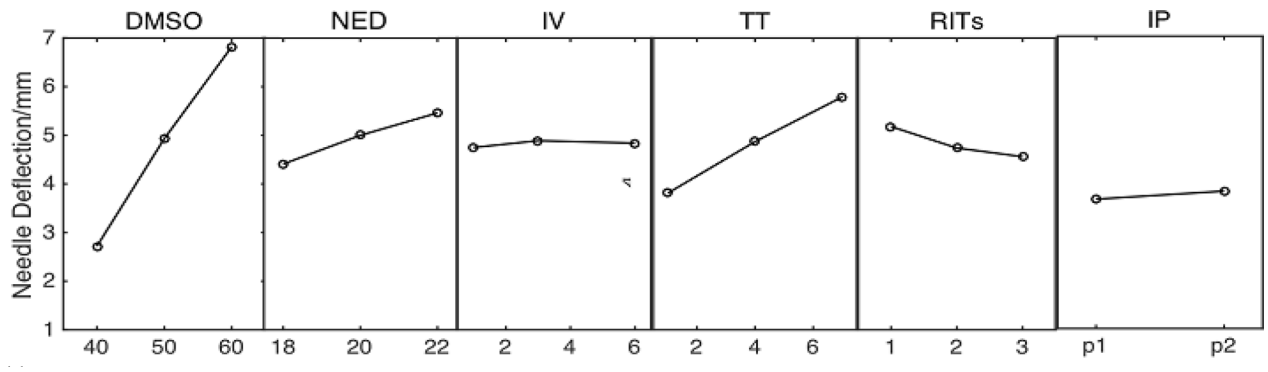

Figure 11 Main effect plot of orthogonal factor on needle deflection

Table 6 Variance analysis on MTD

Source	DOF	SS	MS	F	SG
DMSO	2	18.908	9.454	6.07	***
TT	2	2.582	1.291	0.83	*
NED	2	14.469	7.234	4.64	**
IV	2	25.525	16.762	8.19	***
RITs	2	22.563	11.282	7.24	***
IP	1	9.357	9.357	6	***
Other	6	9.352	1.559	–	–
Total error	17	102.756	–	–	–

Table 7 Variance analysis on MND

Source	DOF	SS	MS	F	SG
DMSO	2	50.700	25.350	73.95	****
TT	2	11.796	5.898	17.2	****
NED	2	3.774	1.887	5.5	***
IV	2	0.0601	0.0301	0.09	*
RITs	2	1.235	0.617	1.8	*
IP	1	0.601	0.601	0.18	*
Other	6	2.057	0.343	–	–
Total error	17	69.683	–	–	–

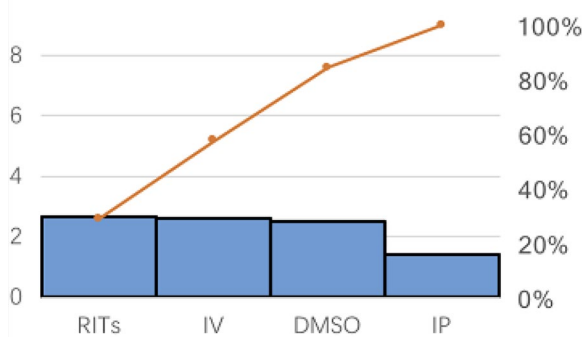

Figure 12 Contributions of the significant factors on MTD

deformation. Differently, the needle deflection are more sensitive to the intrinsic properties of needle and phantom. Hence, the factors related to the phantom stiffness such as the TT should be taken care of if high precision is required for MND.

5 Discussion

According to the comprehensive results of range calculation, the main effect plot and variance analysis, we found that: in the experimental setting range, the three of the most sensitive parameters on maximum tissue deformation(MTD) in the range calculation are RITs (2.68 mm), IV(2.62 mm) and DMSO (2.50 mm). In variance analysis, the most important factors on maximum tissue deformation (MTD) are IV, followed by RITs, DMSO and IP. And NED and TT have nearly no significant impact on MTD. The RITs is firstly emphasized. A second and third insertion into the same trajectory of the phantom would result in larger phantom deformation compared to the first insertion results. It may due to changes in interaction force or internal microstructure altered by the previous insertion. Hence, it is suggested to avoid a repeated insertion in the same location for either the parameter estimation of high accuracy or reduce phantom deformations. In addition, a lower insertion velocity can also reduce the phantom deformation.

Different from the phantom deformation, the three of the major parameters on needle deflection are DMSO (4.11 mm), TT (1.98 mm) and NED (1.05 mm). In variance analysis, the significant sequence on maximum needle deflection (MND) is as follows: DMSO, TT and NED. Other factors should not be considered as inapparent factors. Needle deflections are more sensitive to the material properties of phantom. Within the experimental settings, the different thawing time of PVA phantom would result in dehydration in different degrees, which would influence the properties of phantom. Although the stiffness difference originated from the thawing time is far less than the phantom originated from proportioning changes, it is emphasized that the thawing time of phantom or tissue is a significant factor for needle deflection. From the aspect of both MTD and MND, the volume percentage of DMSO have a great effect on both MTD (rank 3) and MND (rank 1), which means tissue's inherent properties play a major role on the deformation results. The harder phantom tends to have smaller deformations and cause larger deflections of needles.

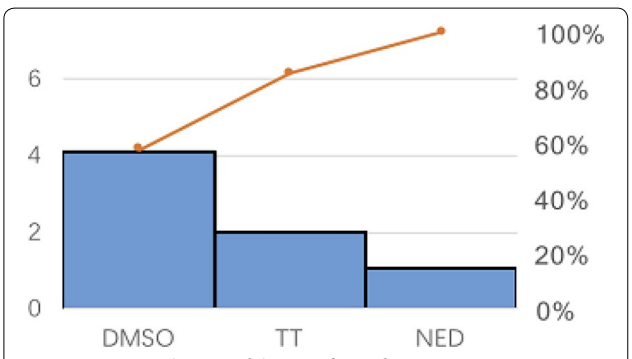

Figure 13 Contribution of the significant factors on MND

6 Conclusions and Future Work

In this paper, the effects of the influential factors on phantom deformations and needle deflections are systematically studied. A global sensitivity analysis is carried out by designing the orthogonal experiments. Six influential factors are classified into three groups: phantom properties, needle properties and the operation parameters. Among these, the repeated insertion times and phantom dehydration time are firstly investigated and studied compared with other conventional factors. The conclusions are as follows:

1. Both the range calculation and variance analysis show the three of the most sensitive parameters on MTD are RITs, IV and DMSO. The results indicate the phantom deformation are more sensitive to the operation factors (RITs and IV). A second and third insertion into the same trajectory of the phantom would result in larger phantom deformation compared to the first insertion results and a lower insertion velocity can also reduce the phantom deformation.
2. The range calculation shows the three of the most sensitive parameters on MND are DMSO, TT and NED. By variance analysis, the significant sequence on maximum needle deflection (MND) is as follows: DMSO, TT and NED. The results indicate the needle deflection is more sensitive to the phantom material properties (DMSO and TT). Especially the thawing time of the phantom has a major effect on the needle deflection by changing the natural material properties of the phantom.
3. From the aspect of both MTD and MND, the volume percentage of DMSO have a great effect on both MTD (rank 3) and MND (rank 1), which means tissue's inherent properties from different organs may cause completely different deformation results. The harder phantom tends to have smaller deformations and cause larger deflections of needles.

The findings of this paper can help researchers in related fields to understand the needle-tissue interaction phenomena and better conduct the needle insertion experiments.

Considering the complexity and financial burden of the experiments, the choice of the influential factors are limited. In the future work, extension studies including factors such as needle tip geometry, phantom constraints would be taken into account.

Acknowledgements
No applicable.

Authors' Contributions
ML discovered the interesting phenomenon on the repeatability of the physical needle insertion experiments, she also designed and conducted the sensitivity experiments to find out the effects of different factors. YL interpreted the experimental results. ML was the major contributor in writing the manuscript. TX assisted with improving the quality of the manuscript. All authors read and approved the final manuscript.

Authors' Information
Murong Li, born in 1994, is currently a PhD candidate at *State Key Laboratory of Fluid Power and Mechatronic Systems, Zhejiang University, Hangzhou, China*. She received her bachelor degree from *Northwest A & F University, China*, in 2016. Her research interests include needle-tissue interaction modeling and needle path planning.

Yong Lei received his PhD degree in mechanical engineering from the *University of Michigan, Ann Arbor, USA*, in 2007. He is a professor in *State Key Laboratory of Fluid Power and Mechatronic Systems, Zhejiang University, China*. His major research interests include fault diagnosis and maintenance in networked systems, modeling and human-machine interfaces design for minimally invasive surgery.

Tian Xu, born in 1994, is currently a PhD candidate at *State Key Laboratory of Fluid Power and Mechatronic Systems, Zhejiang University, China*. He received his bachelor degree from *Zhejiang University, China*, in 2017. His research interests include biomechanical model and inverse problem.

Funding
Supported by Zhejiang Provincial Natural Science Foundation of China (Grant No. LSD19H180004), National Major Scientific Research Instrument Development Project of China (Grant No. 81827804), and Science Fund for Creative Group of NSFC (Grant No. 51821903).

Competing Interests
The authors declare no competing financial interests.

Received: 14 October 2019 Revised: 8 November 2020 Accepted: 18 November 2020
Published online: 09 December 2020

References

[1] N J Berg, J Dankelman, J J Dobbelsteen. Endpoint accuracy in manual control of a steerable needle. *Journal of Vascular and Interventional Radiology*, 2017, 28(2): 276-283.
[2] S G Ullrich, O Grottke, R Rossaint, et al. Virtual needle simulation with haptics for regional anaesthesia. *IEEE Virtual Reality*, 2010, 52(7): 1-3.
[3] A Illanes, B Axel. Novel clinical device tracking and tissue event characterization using proximally placed audio signal acquisition and processing. *Scientific Reports*, 2018, 8(1): 12070.
[4] M Scali, T P Pusch, P Breedveld, et al. Needle-like instruments for steering through solid organs: A review of the scientific and patent literature. *Proceedings of the Institution of Mechanical Engineers Part H Journal of Engineering in Medicine*, 2017, 231(3): 250-265.
[5] Z Tan, D Dini, R Y B Ferdinando, et al. Composite hydrogel: A high fidelity soft tissue mimic for surgery. *Materials & Design*, 2018, 160(12): 886-894.
[6] T L de Jong, L H Pluymen, D J van Gerwen, et al. PVA matches human liver in needle-tissue interaction. *Journal of the Mechanical Behavior of Biomedical Materials*, 2017(69): 223-228.
[7] A Leibinger, A E Forte, Z Tan, et al. Soft tissue phantoms for realistic needle insertion: A comparative study. *Annals of Biomedical Engineering*, 2016, 44(8): 2442-2452.
[8] N V Datla, B Konh, J J Y Koo, et al. Polyacrylamide phantom for self-actuating needle–tissue interaction studies. *Medical Engineering & Physics*, 2014, 36(8): 140-145.
[9] M Kuroda, H Kato, K Hanamoto, et al. Development of a new hybrid gel phantom using carrageenan and gellan gum for visualizing

three-dimensional temperature distribution during hyperthermia and radiofrequency ablation. *International Journal of Oncology*, 2012, 27(1): 175-184.
[10] M Lazebnik, E L Madsen, G R Frank, et al. Tissue-mimicking phantom materials for narrowband and ultrawideband microwave applications. *Physics in Medicine & Biology*, 2005, 50(18): 4245-58.
[11] K B Reed, A M Okamura, N J Cowan. Controlling a robotically steered needle in the presence of torsional friction. *IEEE International Conference on Robotics & Automation*, 2009, No. 5152749.
[12] O A Shergold, N A Fleck. Experimental investigation into the deep penetration of soft solids by sharp and blunt punches, with application to the piercing of skin. *Journal of Biomechanical Engineering*, 2005, 127(5): 838-848.
[13] K J M Surry, H J B Austin, A Fenster, et al. Poly(vinyl alcohol) cryogel phantoms for use in ultrasound and MR imaging. *Physics in Medicine & Biology*, 2004, 49(24): 5529-5546.
[14] S Jiang, S Liu, W Feng. PVA hydrogel properties for biomedical application. *Journal of the Mechanical Behavior of Biomedical Materials*, 2011, 4(7): 1228-1233.
[15] S Eslah, H Tavanai, M Morshed, et al. Electrospinning and characterization of polyvinyl alcohol sericin nanofibers as a potential for tissue engineering applications. *Journal of the Textile Institute Proceedings & Abstracts*, 2015, 107(8): 949-957.
[16] I Mano, H Goshima, M Nambu, et al. New polyvinyl alcohol gel material for MRI phantoms. *Magnetic Resonance in Medicine*, 2010, 3(6): 921-926.
[17] A Haddadi, K Hashtrudi-Zaad. Development of a dynamic model for bevel-tip flexible needle insertion into soft tissues. *Annual International Conference of the IEEE Engineering in Medicine and Biology Society*, 2011: 7478-7482.
[18] P Kim, S Kim, S H Choi, et al. Force modeling for incision surgery into tissue with haptic application. *Smart Structures and Materials Nondestructive Evaluation and Health Monitoring, International Society for Optics and Photonics*, 2015(04): 94311N.
[19] K Kaiguo, P Podder, L Li, et al. A real-time prostate cancer detection technique using needle insertion force and patient-specific criteria during percutaneous intervention. *Medical Physics*, 2009, 36, https://doi.org/10.1118/1.3213453.
[20] Y Chong, X Yu, L Shuang, et al. Force modeling, identification, and feedback control of robot-assisted needle insertion: A survey of the literature. *Sensors*, 2018, 18(2): 561.
[21] D J Gerwen, J Dankelman, J J Dobbelsteen. Needle–tissue interaction forces–A survey of experimental data. *Medical Engineering & Physics*, 2012, 34(6): 665-680.
[22] S Jiang, P Li, Y Yu, et al. Experimental study of needle–tissue interaction forces: Effect of needle geometries, insertion methods and tissue characteristics. *Journal of Biomechanics*, 2014, 47(13): 3344-3353.
[23] D B Van, D T Jong, G D Van, et al. The influence of tip shape on bending force during needle insertion. *Sentific Reports*, 2017, 7(11): 40477.
[24] L Hiemenz, D Stredney, P Schmalbrock. Development of the force-feedback model for an epidural needle insertion simulator. *Stud Health Technol. Inform.*, 1998, 50: 272-277.
[25] H Saito, T Togawa. Detection of needle puncture to blood vessel using puncture force measurement. *Medical & Biological Engineering & Computing*, 2005, 43(2): 240-244.
[26] R Alterovitz, K Goldberg, J Pouliot, et al. Needle insertion and radioactive seed implantation in human tissues: Simulation and sensitivity analysis. *IEEE International Conference on Robotics & Automation*, 2003, 2: 1793-1799.
[27] S Misra, K J Macura, K T Ramesh, et al. The importance of organ geometry and boundary constraints for planning of medical interventions. *Medical Engineering & Physics*, 2009, 31(2): 195-206.
[28] S Misra, K B Reed, K T Ramesh, et al. Observations of needle-tissue interactions. *International Conference of the IEEE Engineering in Medicine & Biology Society*, 2009: 262-265. https://doi.org/10.1109/iembs.2009.5332872.
[29] P J Swaney, J Burgner, H B Gilbert, et al. A flexure-based steerable needle: High curvature with reduced tissue damage. *IEEE Transactions on Biomedical Engineering*, 2013, 60(4): 906-909.
[30] M Mahvash, P E Dupont. Mechanics of dynamic needle insertion into a biological material. *IEEE Transactions on Bio-Medical Engineering*, 2010, 57(4): 934.
[31] D J Van Gerwen. *Needle-tissue interaction by experiment*. Delft University of Technology, 2013: http://resolver.tudelft.nl/uuid:c2dac8ee-0529-49ae-8374-.2d49efd0ba90.
[32] M Li, Y Lei. Repeatability assessment and sensitivity analysis of needle insertion physical experiment. *ASME 2018 13th International Manufacturing Science and Engineering Conference*, 2018, 1: UNSP V001T05A005.
[33] Z Zhang. A flexible new technique for camera calibration. *IEEE Transactions on Pattern Analysis and Machine Intelligence*, 2000, 22(11): 1330-1334.